

LETTERS

Natural allelic variation underlying a major fitness trade-off in *Arabidopsis thaliana*

Marco Todesco^{1*}, Sureshkumar Balasubramanian^{1*†}, Tina T. Hu^{2†}, M. Brian Traw³, Matthew Horton⁴, Petra Epple⁵, Christine Kuhns^{6,7}, Sridevi Sureshkumar^{1†}, Christopher Schwartz^{8,9}, Christa Lanz¹, Roosa A. E. Laitinen¹, Yu Huang², Joanne Chory^{8,10}, Volker Lipka^{6,7}, Justin O. Borevitz⁴, Jeffery L. Dangl^{5,11}, Joy Bergelson⁴, Magnus Nordborg^{2,12} & Detlef Weigel¹

Plants can defend themselves against a wide array of enemies, from microbes to large animals, yet there is great variability in the effectiveness of such defences, both within and between species. Some of this variation can be explained by conflicting pressures from pathogens with different modes of attack¹. A second explanation comes from an evolutionary ‘tug of war’, in which pathogens adapt to evade detection, until the plant has evolved new recognition capabilities for pathogen invasion^{2–5}. If selection is, however, sufficiently strong, susceptible hosts should remain rare. That this is not the case is best explained by costs incurred from constitutive defences in a pest-free environment^{6–11}. Using a combination of forward genetics and genome-wide association analyses, we demonstrate that allelic diversity at a single locus, ACCELERATED CELL DEATH 6 (*ACD6*)^{12,13}, underpins marked pleiotropic differences in both vegetative growth and resistance to microbial infection and herbivory among natural *Arabidopsis thaliana* strains. A hyperactive *ACD6* allele, compared to the reference allele, strongly enhances resistance to a broad range of pathogens from different phyla, but at the same time slows the production of new leaves and greatly reduces the biomass of mature leaves. This allele segregates at intermediate frequency both throughout the worldwide range of *A. thaliana* and within local populations, consistent with this allele providing substantial fitness benefits despite its marked impact on growth.

A survey of *A. thaliana* accessions collected from the wild revealed extensive environment-dependent variation for leaf initiation rate (Supplementary Table 1). One of the strains, Est-1, which produced leaves more slowly than the Col-0 reference strain, also developed extensive necrosis on fully expanded leaves (Fig. 1a, b). Using a recombinant inbred line (RIL) population¹⁴, we identified single major-effect quantitative trait loci (QTL) for both leaf initiation rate and late-onset leaf necrosis (Fig. 1c), with the Est-1 alleles acting in a semi-dominant manner. We fine-mapped both QTL to the same 12-kilobase (kb) region (Supplementary Fig. 1). We targeted the four protein-coding genes in this interval—At4g14400, At4g14410, At4g14420 and At4g14430—with artificial microRNAs (amiRNAs)¹⁵. Knocking down At4g14400, previously identified as ACCELERATED CELL DEATH6 (*ACD6*)¹², suppressed late-onset necrosis and accelerated leaf initiation in Est-1 (Fig. 1a, b and Supplementary Fig. 2a),

whereas downregulation of the other three genes had no visible effects. We also transformed *acd6-2* loss-of-function plants in the Col-0

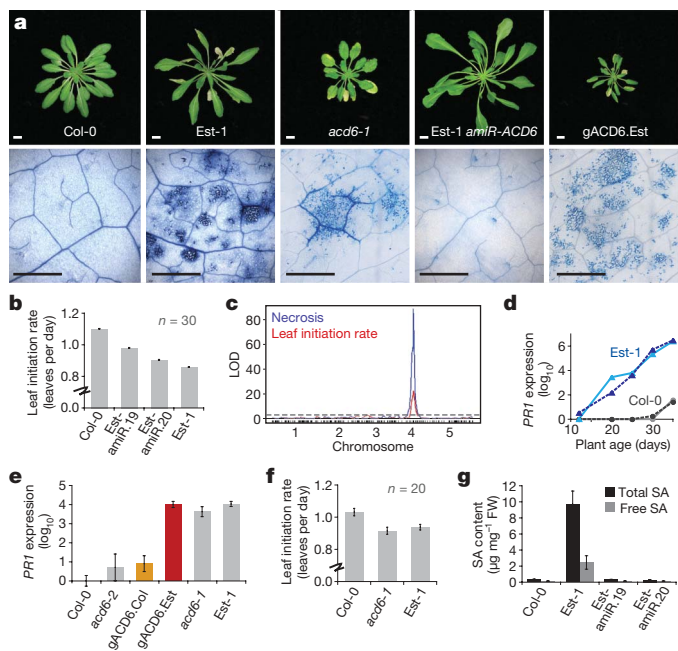


Figure 1 | Identification of a natural *ACD6* allele affecting growth and defence traits. **a**, Top: rosettes of 6-week-old plants. Bottom: close-up of twelfth leaf, stained with Trypan blue for dead cells. *gACD6.Est* is an *acd6-2* mutant in Col-0 (which is morphologically normal; Supplementary Fig. 3) transformed with an Est-1 genomic fragment. Scale bars: 1 cm (top); 1 mm (bottom). **b**, Leaf initiation rates. **c**, QTL maps. The dashed black line indicates significance threshold; ticks indicate positions of genetic markers¹⁴. LOD, logarithm of odds. **d**, *PR1* expression in the sixth leaf (two biological replicates each), normalized to those in 12-day-old Est-1 plants. **e**, *PR1* expression in different genotypes. **f**, Leaf initiation rates. **g**, SA content in the sixth leaf of 35-day-old plants. Only wild-type Est-1 was significantly different from any of the other lines ($P < 0.005$). The 35S:amiR-*ACD6* construct had no effect on SA levels in Col-0. FW, fresh weight. Standard errors are indicated in panels **b**, **e–g**.

¹Department of Molecular Biology, Max Planck Institute for Developmental Biology, 72076 Tübingen, Germany. ²Molecular and Computational Biology, University of Southern California, Los Angeles, California 90089, USA. ³Department of Biological Sciences, University of Pittsburgh, Pittsburgh, Pennsylvania 15238, USA. ⁴Department of Ecology and Evolution, University of Chicago, Chicago, Illinois 60637, USA. ⁵Department of Biology, University of North Carolina, Chapel Hill, North Carolina 27599, USA. ⁶The Sainsbury Laboratory, John Innes Centre, Colney, Norwich NR4 7UH, UK. ⁷Albrecht von Haller Institute for Plant Sciences, Georg August University Göttingen, 37073 Göttingen, Germany. ⁸Plant Biology Laboratory, The Salk Institute for Biological Studies, La Jolla, California 92037, USA. ⁹Department of Biochemistry, University of Wisconsin, Madison, Wisconsin 53706, USA. ¹⁰Howard Hughes Medical Institute, The Salk Institute for Biological Studies, La Jolla, California 92037, USA. ¹¹Department of Microbiology and Immunology, Curriculum in Genetics and Carolina Center for Genome Sciences, University of North Carolina, Chapel Hill, North Carolina 27599, USA. ¹²Gregor Mendel Institute, 1030 Vienna, Austria. [†]Present addresses: School of Biological Sciences, University of Queensland, St Lucia, Queensland 4072, Australia (S.B., S.S.); Lewis-Sigler Institute, Princeton University, Princeton, New Jersey 08544, USA (T.T.H.).

*These authors contributed equally to this work.

background with an *ACD6* genomic fragment from Est-1, and found that these plants suffered from late-onset necrosis (Fig. 1a). This was not the case when we used a Col-0 genomic fragment (Supplementary Fig. 3a). Thus, *ACD6* is responsible for the leaf initiation and necrosis QTL.

ACD6 encodes a transmembrane protein with cytosolic ankyrin repeats^{12,13}. An ethylmethane-sulphonate-induced gain-of-function allele in Col-0, *acd6-1*, which carries a single amino-acid change in the transmembrane domain^{12,16}, is characterized by spontaneous cell death. In *acd6-1* and several other so-called lesion mimic mutants, this is associated with constitutive activation of defence pathways and increased resistance to microbial infection¹⁷, although the relationship between cell death and disease resistance is complex. Local cell death, known as the hypersensitive response, is a common consequence of pathogen recognition by genotypes with inducible immunity¹⁸. Not all lesion-mimic mutants, however, are more resistant to pathogen attack than wild type¹⁷, and effective disease resistance is largely uncoupled from cell death in *disease no death* 1 mutants¹⁹.

Similar to *acd6-1* mutants, Est-1 plants had macroscopic lesions and microscopic cell death (Fig. 1a). Furthermore, like *acd6-1*, *PR1* and other genes mediating the response to biotic stresses were expressed much more highly in Est-1 than in Col-0 wild-type plants, and this was reproduced by transforming the Est-1 allele of *ACD6* into *acd6-2* loss-of-function mutants in the Col-0 background (Fig. 1d, e and Supplementary Fig. 2b). Conversely, *acd6-1* mutants produced leaves more slowly than wild-type Col-0, thus mimicking Est-1 (Fig. 1f). *ACD6* acts in a feed-forward loop that regulates the accumulation of salicylic acid (SA), a key molecule in pathogen defence signalling^{13,16}. Accordingly, conversion of SA to catechol by transgenic expression of the bacterial salicylate hydroxylase gene *nahG* (ref. 20) strongly attenuates *acd6-1* phenotypes^{12,16,21}. Est-1 plants had higher SA levels than Col-0 plants, and these were strongly reduced by knocking down *ACD6* (Fig. 1g). As for *acd6-1*, *nahG* expression suppressed necrosis in Est-1 (Supplementary Fig. 4).

ACD6 RNA expression in leaves increased with age, with *ACD6* levels rising earlier in Est-1 than in Col-0 (Supplementary Fig. 2c). *PR1* expression followed a similar profile only in Est-1 (Fig. 1d). *PR1* levels in Est-1 were reduced after knockdown of *ACD6* with the *amiR-ACD6* construct (Supplementary Fig. 2d). Conversely, *PR1* expression in *acd6-2* loss-of-function mutants transformed with an Est-1 genomic fragment was three orders of magnitude higher than in *acd6-2* transformed with a Col-0 fragment, despite similar *ACD6* levels (Fig. 1e and Supplementary Fig. 3b). The Col-0 and Est-1 proteins differ at 24 out of 670 amino acids (Supplementary Fig. 5). Expressing *ACD6* coding sequences from Est-1 under control of the Col-0 promoter was sufficient to produce an Est-1-like phenotype in *acd6-2* mutants, whereas the opposite configuration did not cause any symptoms (Supplementary Fig. 6). We conclude that changes in the protein sequence explain much of the differences in *ACD6* activity between Est-1 and Col-0, which was further confirmed by expressing both alleles from a foreign promoter (Supplementary Fig. 2e, f).

acd6-1 plants not only have necrotic lesions, but they are also small^{12,16,21}. Both the *amiR-ACD6* transgene and *nahG* expression caused a marked increase, of more than 50%, in the dry weight of Est-1 leaves. The difference between wild-type and 35S::*amiR-ACD6* or 35S::*nahG* Est-1 plants was similar to that between *acd6-1* and its Col-0 parent. In contrast, the 35S::*amiR-ACD6* and 35S::*nahG* transgenes had only minor effects on Col-0 (Fig. 2a). Similarly, introduction of the Est-1 allele, but not the Col-0 *ACD6* allele, into *acd6-2* loss-of-function mutants strongly reduced leaf weight (Supplementary Fig. 3c). Altered *ACD6* activity in Est-1 thus has additive effects on total biomass, by slowing the rate at which new leaves are produced and by limiting the final size of individual leaves.

acd6-1 mutants display enhanced resistance to *Pseudomonas syringae* pv. *tomato* DC3000, a hemi-biotrophic pathogen¹⁶. We isolated a biotrophic fungus, powdery mildew *Golovinomyces orontii* T1,

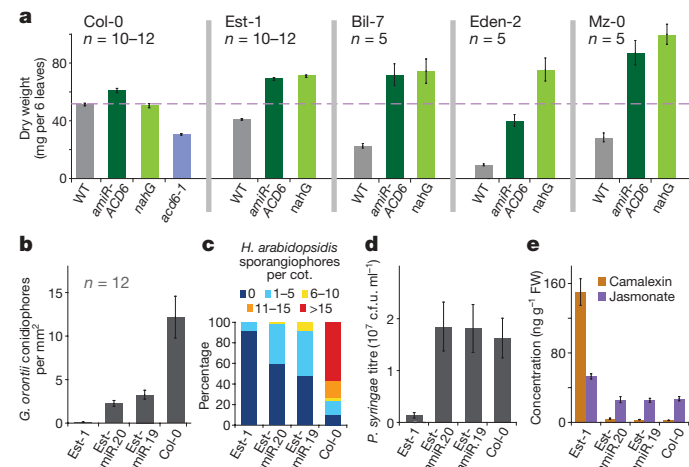


Figure 2 | Effects of a natural *ACD6* allele on leaf biomass, pathogen susceptibility and metabolite content. **a**, Leaf biomass. The difference between wild-type and transgenic lines was significant for all accessions but Col-0 ($P < 0.001$). **b**, *G. orontii* T1 conidiophores on 4-week-old plants, 5 days post inoculation (d.p.i.). **c**, *H. arabidopsis* Noco2 sporangiophores on 2-week-old seedlings (5 d.p.i.). cot., cotyledon. **d**, *P. syringae* DC3000 growth. 35S::*amiR-ACD6* did not affect susceptibility of Col-0. **e**, Camalexin and jasmonate concentrations. The difference between Est-1 and the other genotypes was significant ($P < 0.005$). Standard errors are indicated in panels **a**, **b**, **d**, **e**.

from spontaneous infections of *A. thaliana* in Tübingen. Est-1 was resistant to this isolate, which easily infected many other accessions including Col-0. Resistance was genetically linked to the *ACD6* region (Supplementary Fig. 1f), and knocking down *ACD6* caused Est-1 to become susceptible to infection by *G. orontii* (Figs 2b and 3a, b). Increased susceptibility of 35S::*amiR-ACD6* Est-1 plants was also seen

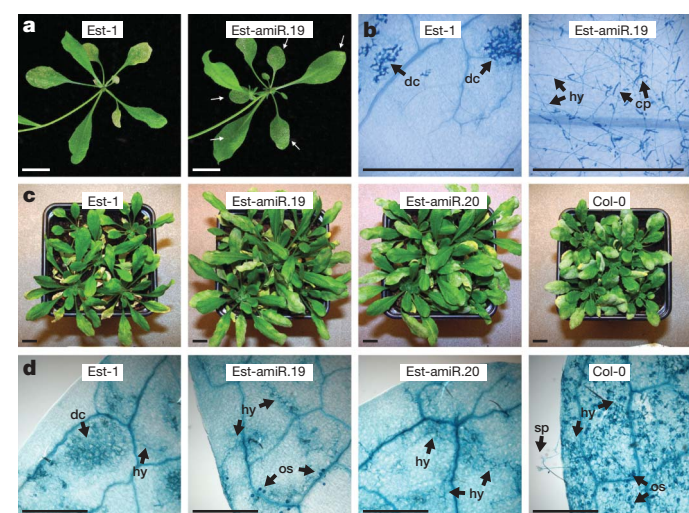


Figure 3 | Effects of a natural *ACD6* allele on pathogen susceptibility. **a**, Infection of 4-week-old plants by *G. orontii* T1 (5 d.p.i.). Arrows indicate fungal growth. **b**, Trypan blue staining of inoculated leaves. Dead plant cells (dc), hyphae (hy) and mature conidiophores (cp) are indicated. **c**, Infection of 6-week-old plants with *G. cichoracearum* UCSC1 (10 d.p.i.). Note the increasing severity of infection symptoms from left to right. **d**, Five-week-old plants inoculated with *H. arabidopsis* Noco2. Trypan blue staining of the fourth leaf (7 d.p.i.) is shown. Hyphal growth (hy), which was seldom observed in Est-1, as well as oosporangia (os) were common in 35S::*amiR-ACD6* Est-1 plants. See Supplementary Fig. 7 for adult leaves. In Col-0, many sporangiophores (sp) were seen. For both powdery and downy mildews, pathogen susceptibility and *ACD6* expression levels in 35S::*amiR-ACD6* lines were correlated (see Supplementary Fig. 2a). Scale bars: 1 cm in **a** and **c**; 1 mm in **b** and **d**.

for *Golovinomyces cichoracearum* UCSC1 (Fig. 3c), and for two other biotrophic pathogens: the downy mildew *Hyaloperonospora arabidopsis* Noco2, an oomycete (Figs 2c and 3d and Supplementary Fig. 7), and the bacterium *P. syringae* DC3000 (Fig. 2d).

Variation in leaf weight associated with differences in SA content is positively correlated with several fitness-related traits, such as seed yield, in *A. thaliana*²². The increased resistance to biotrophic pathogens conditioned by the Est-1 allele of *ACD6* indicates that this allele can provide environment-dependent fitness advantages and may therefore not be rare, despite its negative effects on biomass. Across

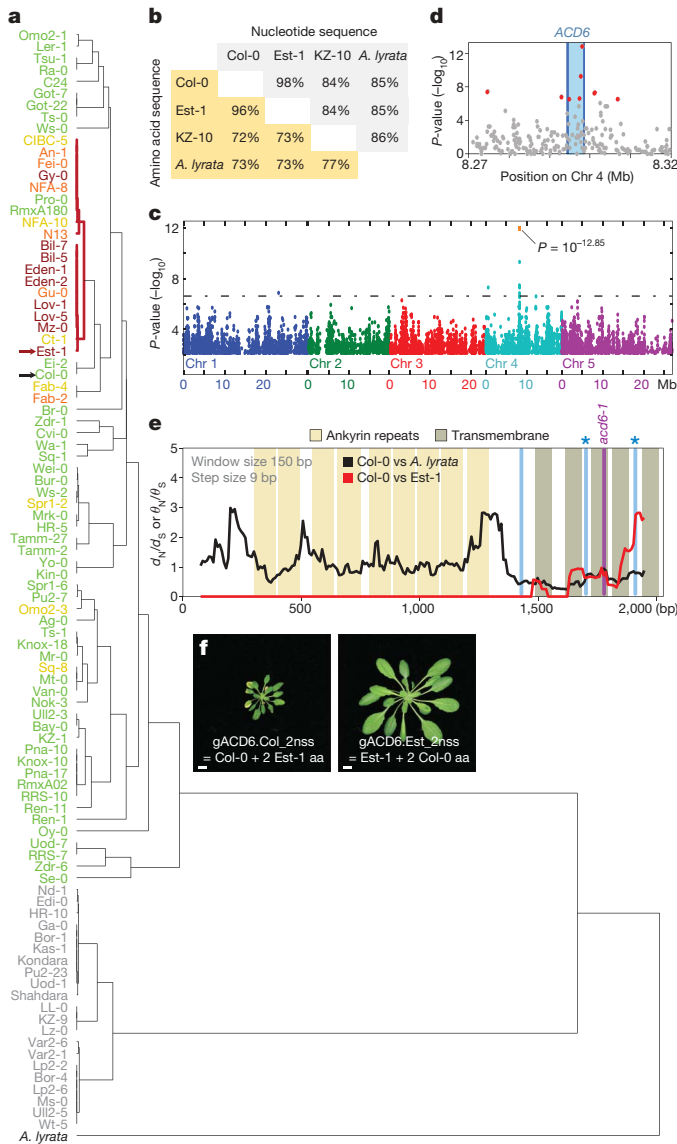


Figure 4 | *ACD6* sequence diversity in *Arabidopsis*. **a**, Hierarchical clustering of *ACD6* alleles. Col-0 and Est-1 are indicated with arrows, and Est-1-like sequences are highlighted. Yellow indicates mild, orange intermediate and red severe late-onset necrosis. KZ-10-like alleles are grey. **b**, Pair-wise identity of *ACD6* alleles. **c**, Whole-genome scan of 216,130 SNPs for association with necrosis across 96 accessions shown in a²⁴. **d**, Genomic region containing 9 of 15 SNPs with lowest *P*-values. **e**, Polymorphism and divergence levels at *ACD6* (see also Supplementary Figs 8 and 10 and Supplementary Table 6). Blue lines indicate non-synonymous SNPs shared among Est-1-like alleles, and Fab-2 and Fab-4 (Supplementary Fig. 5). The two causal SNPs (see f) are indicated by asterisks, as is the *acd6-1* mutation. d_N , rate of non-synonymous substitutions; d_S , rate of synonymous substitutions. **f**, Six-week-old *acd6-2* plants transformed with modified genomic clones of *ACD6*, in which two codons were swapped between Est-1 and Col-0. See also Supplementary Fig. 6. Compare to Fig. 1a and Supplementary Fig. 3a for unmutated versions. Scale bars: 1 cm.

96 strains from throughout the worldwide range of *A. thaliana*²³, 71 accessions had *ACD6* alleles similar to those of Est-1 and Col-0 (Fig. 4a). The 73 strains featured a total of 141 non-synonymous substitutions, of which 67 were located in the ankyrin repeats and 17 in the predicted transmembrane domains (Supplementary Figs 5 and 8a, b). Most of the remaining strains had an *ACD6* allele, exemplified by KZ-10 that was as divergent from the Col-0 reference allele as it was from the MN47 strain of *Arabidopsis lyrata* (Fig. 4a, b). The relationship among the three alleles as well as At4g14390, a homologue immediately upstream of *ACD6*, is complex, and might involve a history of gene conversion.

Eighteen accessions shared *ACD6* sequences closely related to the Est-1-like allele. All except two of these strains suffered from symptoms similar to Est-1, whereas necrosis was rare among the other 77 strains (Figs 4a and 5a, Supplementary Fig. 9a and Supplementary Table 2). These observations are consistent with the identification of the *ACD6* region in a genome-wide association scan for loci causing necrosis in the same set of 96 accessions²⁴. Nine of the fifteen single nucleotide polymorphisms (SNPs) with the lowest *P*-values in the genome-wide scan were within or next to *ACD6* (Fig. 4c, d). The predominance of the peak near *ACD6* in the genome-wide scan demonstrates that allelic variation at this locus is the major determinant of global variation for this trait.

The group of Est-1-like alleles shared three non-synonymous substitutions in the transmembrane region (Fig. 4e and Supplementary Figs 5 and 8a, b). This region also stood out because of its excess of non-synonymous over synonymous substitutions between Col-0 and Est-1, which contrasts with this segment being highly conserved in an interspecific comparison (Fig. 4e and Supplementary Figs 8c, d and 10). An exchange of two of these non-synonymous substitutions between Est-1 and Col-0 genomic clones demonstrated that they were both necessary and sufficient for strong late-onset necrosis and activation of immune reactions (Fig. 4f and Supplementary Fig. 6b, c).

We crossed several Est-1-like accessions to the Col-0 reference strain, and confirmed in *F*₂ populations that *ACD6* co-segregated with necrosis (Supplementary Table 2). Both reduction of SA using the 35S::*nahG* transgene and amiRNA-mediated knockdown of *ACD6*

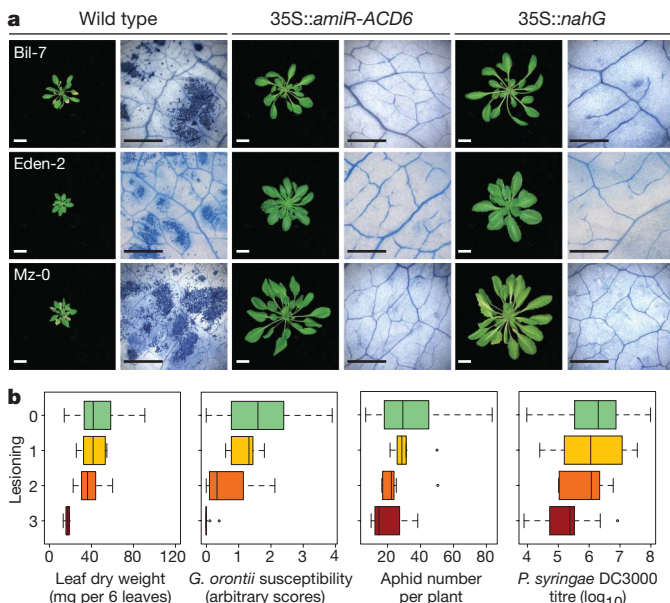


Figure 5 | Correlation between late-onset necrosis, growth and defence traits. **a**, Late-onset necrosis in accessions with an Est-1-like *ACD6* allele is suppressed by 35S::*amiR-ACD6*, or by *nahG*-mediated SA depletion. See Supplementary Fig. 9 for additional accessions. Scale bars: 2 cm for rosettes; 1 mm for micrographs. **b**, Correlation between late-onset necrosis and different traits across 96 accessions used for genome-wide association studies²⁴. Lesioning scores reflect the range of symptoms indicated in Fig. 4a.

suppressed late-onset necrosis and increased leaf biomass in several strains (Figs 2a and 5a, Supplementary Fig. 9 and Supplementary Table 2), confirming increased activity of *ACD6* in these accessions.

We have shown that the Est-1-like *ACD6* allele has marked effects on leaf biomass, late-onset necrosis and pathogen susceptibility. In the collection of 96 strains, we observed strong negative correlation of late-onset necrosis not only with leaf biomass, but also with resistance to *G. orontii* T1 and *P. syringae* DC3000, and with the extent to which proliferation of the aphid *Myzus persicae* was supported (Fig. 5b). Interestingly, whereas SNPs in the *ACD6* region were strongly associated with necrosis in a genome-wide scan, associations with leaf biomass as well as *G. orontii* and *M. persicae* resistance were much weaker, and not significant at all for DC3000 growth²⁴ (Supplementary Tables 3, 4 and 5). Including necrosis as a co-factor in genome-wide scans revealed additional associations outside the *ACD6* region (Supplementary Fig. 11), indicating that other factors can mask the effects of *ACD6* on disease resistance.

Despite the strong sequence differentiation between *ACD6* alleles, there is no obvious geographic structure to their distribution, and F_{ST} values do not deviate from the genome-wide pattern²³ (Supplementary Fig. 12). We also analysed a local collection of 890 *A. thaliana* individuals representing 202 distinct multi-locus genotypes from the Tübingen region²⁵. All three allele types defined by function or sequence—Col-0-like, Est-1-like and KZ-10-like—were present throughout the region, and often co-occurred (Supplementary Fig. 13). It therefore seems that evolutionary forces maintain allelic variation at *ACD6* both across the global range of *A. thaliana* and within local populations.

Fitness costs imposed by activation of defence have often been proposed as a possible explanation for genetic variation in disease resistance⁶, and costs associated with individual genes have been detected in field trials^{9–11}. Specifically, priming of SA-related defence responses significantly increases disease resistance and plant fitness in the field²⁶, but reduces fitness in the absence of pathogens²². The developmentally regulated activation of *ACD6* and downstream defence components in wild *A. thaliana* strains carrying the hyper-active *ACD6* allele (Fig. 1d and Supplementary Fig. 2c) could induce a similar primed state.

The positive association between necrosis and reduced susceptibility to many different microbes—including bacteria, oomycetes and fungi—and at least some insects is remarkable. Effectiveness of the Est-1 allele of *ACD6* against such a wide range of enemies is probably due to elevated levels of SA (Fig. 1g), and to the antimicrobial compound camalexin, which is moderately increased in *acd6-1* mutants¹⁶, as well as another defence hormone, jasmonate (Fig. 2e). In this context, it is interesting that the effects of knocking down *ACD6* in different accessions varied (Fig. 2a, 5a; Supplementary Fig. 9), indicating that there is a suite of genetic factors that modulate and fine-tune *ACD6* activity.

The co-occurrence of functionally distinct alleles across both global and local populations of *A. thaliana* is consistent with this locus being under balancing selection, a pattern often seen for conventional disease resistance (*R*) genes²⁷. What sets *ACD6* apart from *R* genes is, however, that the latter confer race-specific disease resistance, whereas *ACD6* protects against a broad spectrum of unrelated enemies and predators. Unusually large benefits, in turn, might make the substantial reduction in vegetative biomass caused by *ACD6* more acceptable. To put it differently, accessions with Est-1-like alleles of *ACD6* seem to pursue an alternative life-history strategy, being small, but well protected, compared to other strains that are larger, but less well prepared to combat pathogens.

METHODS SUMMARY

The *acd6-1* mutant¹⁶ and the recombinant inbred line (RIL) population¹⁴ have been described previously; the *acd6-2* T-DNA insertion line was from the Salk collection²⁸. QTL analysis was done using the R-qt package²⁹ implemented in R (<http://www.r-project.org>). For fine mapping, we combined information from

an F₂ population between Col-0 and Est-1 with the heterogeneous inbred family (HIF) strategy³⁰.

Unless otherwise stated, plants were grown under short days (8 or 9 h light). For phenotypic assays and pathotesting, a randomized design was used. For pathogen testing with *G. orontii* T1, plants were grown on soil under in a greenhouse at 21–23 °C; for *G. cichoracearum* UCSC1, in a phytochamber at 20 °C and 60% humidity; for *H. arabidopsis* Noco2, in a phytochamber at 22 °C during the day and 18 °C during the night. For *P. syringae* pv. tomato DC3000 and the common peach aphid *Myzus persicae*, plants were grown on soil in a phytochamber at 20 °C, 12 h light. Metabolites were measured using previously published methods (see Methods).

Full Methods and any associated references are available in the online version of the paper at www.nature.com/nature.

Received 10 July 2009; accepted 14 April 2010.

- Glazebrook, J. Contrasting mechanisms of defense against biotrophic and necrotrophic pathogens. *Annu. Rev. Phytopathol.* **43**, 205–227 (2005).
- Holub, E. B. The arms race is ancient history in *Arabidopsis*, the wildflower. *Nature Rev. Genet.* **2**, 516–527 (2001).
- Holub, E. B. Natural variation in innate immunity of a pioneer species. *Curr. Opin. Plant Biol.* **10**, 415–424 (2007).
- Jones, J. D. & Dangl, J. L. The plant immune system. *Nature* **444**, 323–329 (2006).
- Bent, A. F. & Mackey, D. Elicitors, effectors, and *R* genes: the new paradigm and a lifetime supply of questions. *Annu. Rev. Phytopathol.* **45**, 399–436 (2007).
- Heil, M. & Baldwin, I. T. Fitness costs of induced resistance: emerging experimental support for a slippery concept. *Trends Plant Sci.* **7**, 61–67 (2002).
- Mauricio, R. Costs of resistance to natural enemies in field populations of the annual plant *Arabidopsis thaliana*. *Am. Nat.* **151**, 20–28 (1998).
- Heil, M., Hilpert, A., Kaiser, W. & Linsenmair, K. E. Reduced growth and seed set following chemical induction of pathogen defence: Does Systemic Acquired Resistance (SAR) incur allocation costs? *J. Ecol.* **88**, 645–654 (2000).
- Tian, D., Traw, M. B., Chen, J. Q., Kreitman, M. & Bergelson, J. Fitness costs of *R*-gene-mediated resistance in *Arabidopsis thaliana*. *Nature* **423**, 74–77 (2003).
- Zavala, J. A. & Baldwin, I. T. Fitness benefits of trypsin proteinase inhibitor expression in *Nicotiana attenuata* are greater than their costs when plants are attacked. *BMC Ecol.* **4**, 11 (2004).
- Korves, T. A novel cost of *R* gene resistance in the presence of disease. *Am. Nat.* **163**, 489–504 (2004).
- Lu, H., Rate, D. N., Song, J. T. & Greenberg, J. T. *ACD6*, a novel ankyrin protein, is a regulator and an effector of salicylic acid signaling in the *Arabidopsis* defense response. *Plant Cell* **15**, 2408–2420 (2003).
- Lu, H., Liu, Y. & Greenberg, J. T. Structure-function analysis of the plasma membrane-localized *Arabidopsis* defense component *ACD6*. *Plant J.* **44**, 798–809 (2005).
- Balasubramanian, S. et al. QTL mapping in new *Arabidopsis thaliana* advanced intercross-recombinant inbred lines. *PLoS ONE* **4**, e4318 (2009).
- Schwab, R., Ossowski, S., Riester, M., Warthmann, N. & Weigel, D. Highly specific gene silencing by artificial microRNAs in *Arabidopsis*. *Plant Cell* **18**, 1121–1133 (2006).
- Rate, D. N., Cuenca, J. V., Bowman, G. R., Guttmann, D. S. & Greenberg, J. T. The gain-of-function *Arabidopsis* *acd6* mutant reveals novel regulation and function of the salicylic acid signaling pathway in controlling cell death, defenses, and cell growth. *Plant Cell* **11**, 1695–1708 (1999).
- Lorrain, S., Vailleau, F., Balague, C. & Roby, D. Lesion mimic mutants: keys for deciphering cell death and defense pathways in plants? *Trends Plant Sci.* **8**, 263–271 (2003).
- Greenberg, J. T. & Yao, N. The role and regulation of programmed cell death in plant-pathogen interactions. *Cell. Microbiol.* **6**, 201–211 (2004).
- Yu, I. C., Parker, J. & Bent, A. F. Gene-for-gene disease resistance without the hypersensitive response in *Arabidopsis dnd1* mutant. *Proc. Natl. Acad. Sci. USA* **95**, 7819–7824 (1998).
- Gaffney, T. et al. Requirement of salicylic acid for the induction of systemic acquired resistance. *Science* **261**, 754–756 (1993).
- Lu, H. et al. Genetic analysis of *acd6-1* reveals complex defense networks and leads to identification of novel defense genes in *Arabidopsis*. *Plant J.* **58**, 401–412 (2009).
- Abreu, M. E. & Munné-Bosch, S. Salicylic acid deficiency in *NahG* transgenic lines and *sid2* mutants increases seed yield in the annual plant *Arabidopsis thaliana*. *J. Exp. Bot.* **60**, 1261–1271 (2009).
- Nordborg, M. et al. The pattern of polymorphism in *Arabidopsis thaliana*. *PLoS Biol.* **3**, e196 (2005).
- Atwell, S. et al. Genome-wide association study of 107 phenotypes in *Arabidopsis thaliana* inbred lines. *Nature*. doi:10.1038/nature08800 (24 March 2010).
- Bomblies, K. et al. Local-scale patterns of genetic variability, outcrossing and spatial structure in natural stands of *Arabidopsis thaliana*. *PLoS Genet.* **6**, e1000890 (2010).
- Traw, M. B., Kniskern, J. M. & Bergelson, J. SAR increases fitness of *Arabidopsis thaliana* in the presence of natural bacterial pathogens. *Evolution* **61**, 2444–2449 (2007).

27. Van der Hoorn, R. A., De Wit, P. J. & Joosten, M. H. Balancing selection favors guarding resistance proteins. *Trends Plant Sci.* **7**, 67–71 (2002).
28. Alonso, J. M. *et al.* Genome-wide insertional mutagenesis of *Arabidopsis thaliana*. *Science* **301**, 653–657 (2003).
29. Broman, K. W., Wu, H., Sen, S. & Churchill, G. A. R/qtl: QTL mapping in experimental crosses. *Bioinformatics* **19**, 889–890 (2003).
30. Tuinstra, M., Ejeta, G. & Goldsbrough, P. Heterogenous inbred family (HIF) analysis: a method for developing near-isogenic lines that differ at quantitative trait loci. *Theor. Appl. Genet.* **95**, 1005–1011 (1997).

Supplementary Information is linked to the online version of the paper at www.nature.com/nature.

Acknowledgements We thank S.-W. Park and D. Klessig for the *nahG* clone; J. Greenberg, the NSF-supported *Arabidopsis* Biological Resource Centre (ABRC) and the European *Arabidopsis* Stock Centre (NASC) for seeds; and S. Atwell, K. Broman and Y.-L. Guo for advice. We are grateful to K. Bomblies and L. Yant for establishing the Tübingen *A. thaliana* collection. This work was supported by NIH NRSA fellowship F23-GM65032-1 (C.S.), an EMBO Long-Term Fellowship (S.B.), NIH grants GM62932 (J.C. and D.W.), GM057171 (J.L.D.), GM057994 (J.B.) and

GM073822 (J.O.B.), NSF grants DEB-0519961 (J.B. and M.N.) and NSF MCB0603515 (J.B.), HFSPO grant RGP0057/2007-C (J.L.D. and D.W.), DFG grant LI 1317/2-1 (V.L.), the Gatsby Foundation (V.L.), the Dropkin Foundation (J.B.), the Howard Hughes Medical Institute (J.C.), Marie Curie RTN SY-STEM (D.W.), ERA-PG (BMBF) grant ARABRAS (D.W.), FP6 IP AGRON-OMICS (contract LSHG-CT-2006-037704, D.W.), a Gottfried Wilhelm Leibniz Award of the DFG (D.W.), and the Max Planck Society (D.W.).

Author Contributions M.T., S.B., J.C., V.L., J.O.B., J.L.D., J.B., M.N. and D.W. conceived the study; M.T., S.B., M.B.T., M.H., P.E., C.K., S.S., C.S., C.L. and R.A.E.L. performed the experiments; M.T., S.B., T.T.H., M.B.T., Y.H., J.B., M.N. and D.W. analysed the data; and M.T., S.B. and D.W. wrote the paper with contributions from all authors.

Author Information DNA sequences have been deposited in GenBank under accession numbers HM053468 and HM053469 and HM214805 to HM214897. Reprints and permissions information is available at www.nature.com/reprints. The authors declare no competing financial interests. Readers are welcome to comment on the online version of this article at www.nature.com/nature. Correspondence and requests for materials should be addressed to D.W. (weigel@weigelworld.org).

METHODS

Plant material. The *acd6-1* mutant¹⁶ and the recombinant inbred line (RIL) population¹⁴ have been described; the *acd6-2* T-DNA insertion line was from the Salk collection²⁸.

Phenotyping and QTL mapping. For phenotypic measurements, a completely randomized design was used. To minimize positional effects, trays were turned every 2 days, and their position in the growth rooms was rotated every 2 days.

Leaf initiation rate was measured by marking the newly developed visible leaves every 2 days. Values reported are averages across the whole life of the plant, and were calculated as $[(l - l_0)/(d_l - d_0)]$, in which d_l is the last day in which the plant produced leaves, d_0 is the first day in which leaves appeared, l is the final leaf number and l_0 is the number of leaves at d_0 (usually two).

As a quantitative indicator of necrosis, we recorded the day on which the extent of yellowing in the sixth true leaf reached approximately 50% of the leaf area.

Leaf biomass was measured on six fully expanded rosette leaves without signs of necrosis, collected from individual 40- to 45-day-old plants. Leaves were weighed after desiccation for 24 h at 85 °C. Inbred strains were arbitrarily divided into four classes (severe, intermediate, mild, absent) according to the onset and extent of necrosis.

For QTL analysis, six plants were grown for each of the 180 RILs¹⁴. QTL analysis was done using the R-qlt package²⁹ implemented in R (<http://www.r-project.org>). For fine mapping, we combined information from an F₂ population between Col-0 and Est-1 with the heterogeneous inbred family (HIF) strategy³⁰. Descendants of RIL48, which was segregating for the interval of interest, were genotyped throughout the interval, to identify new recombinants. In addition to microsatellite markers, predicted SNPs (<http://polymorph.weigelworld.org>) were exploited for marker design (Supplementary Table 7a). Genotyping of HIF48 plants with an additional 311 markers³¹ confirmed that these plants were otherwise homozygous across the rest of the genome. The leaf initiation rate QTL was fine-mapped through progeny testing of the plants used for mapping the necrosis QTL. For each line, 10 plants fixed for the Col-0 allele and 10 fixed for the Est-1 allele were phenotyped.

Tukey-Kramer tests were used to determine significance for multiple comparisons.

Histology. Trypan blue (Sigma-Aldrich) staining was performed as described³².

Transgenes and expression assays. Three artificial miRNAs each for At4g14400, At4g14410, At4g14420 and At4g14430 (Supplementary Table 8) were designed using the WMD online tool (<http://wmd.weigelworld.org/>)³³ against sequences conserved between Col-0 and Est-1, and cloned into the pRS300 vector. A *nahG* clone was a gift from S.-W. Park and D. Klessig. Artificial miRNAs, the *nahG* open reading frame and the *ACD6* cDNAs were placed under control of the constitutive CaMV 35S promoter in pFK210 derived from pGREEN (ref. 34). Genomic fragments containing the entire non-coding region upstream of *ACD6*, the transcribed sequences and 500 bp or more of downstream sequences from Col-0, Est-1 and *acd6-1* were cloned into pFK202, a pGREEN-derived binary vector. To exchange the promoter regions, the clones were restricted at a BspEI site. Non-synonymous substitutions affecting amino acids at position 566 and 634 of the *ACD6* reference protein were introduced by PCR-mediated mutagenesis in both the Col-0 and Est-1 genomic construct. Constructs were introduced into plants by *Agrobacterium tumefaciens*-mediated transformation³⁵. The *acd6-2* (N545869) T-DNA insertion line from the Salk collection²⁸ was obtained from the European *Arabidopsis* Stock Centre (NASC).

Quantitative reverse transcription PCR (qRT-PCR) assays were performed as described³⁶, using RNA extracted from the sixth leaf of 6-week-old plants, unless otherwise stated. Expression levels were normalized against β-tubulin 2 (At5g62690). An experimentally quantified average amplification efficiency of 1.98 was used in the calculations. Primers used for qRT-PCR are given in Supplementary Table 9.

Sequencing of *ACD6*. Fragments of about 1 kb in length covering the *ACD6* region were PCR amplified, and pooled products from two independent PCR reactions were sequenced. For KZ-10, which belongs to the same haplogroup as KZ-9 (<http://arabidopsis.usc.edu/Accession/haploGroup/58>)³⁷, a fosmid library was prepared using the CopyControl Fosmid Library Production Kit (Epicentre Biotechnologies), according to the manufacturer's instructions. The library was screened using probes corresponding to sequences upstream and downstream of *ACD6* in Col-0. A fosmid containing the entire *ACD6* region was shotgun sequenced; individual sequences were assembled using SeqMan (DNAStar). *ACD6* sequences from Col-0, Est-1, KZ-10 and *Arabidopsis lyrata* MN47 were aligned using ClustalW version 2 (ref. 38). Coordinates reflect TAIR8 annotation.

Population genetic analyses. Sequences were aligned using both PAL2NAL³⁹ and MUSCLE⁴⁰. The subsequent alignments were then inspected visually and edited as necessary. Population genetic summary statistics were computed using

code based on the libsequence package⁴¹. Divergence at synonymous and non-synonymous sites (d_S , d_N) was estimated using PAML⁴². Trees were computed and plotted using PhyML under the R package ape (ref. 43).

Segregation analysis in F₂ populations. Nine accessions with late-onset necrosis (Supplementary Table 2) were crossed to the reference strain Col-0. Between 120 and 240 F₂ plants from each cross were phenotyped for presence and severity of necrosis, using an arbitrary scale from 0 (absence of necrosis) to 4 (severe necrosis). These plants were then genotyped using a marker that distinguishes Est-1-like alleles from the Col-0 allele of *ACD6* (Supplementary Table 7b).

Pathogen testing. A local isolate of powdery mildew occurring on *A. thaliana* plants in Tübingen was identified as *G. orontii* through analysis of the sequence of ribosomal DNA internal transcribed spacers (rDNA ITS)⁴⁴. For inoculation, leaves from heavily infected *A. thaliana* plants were passed repeatedly over pots of 3-week-old plants to spread the fungal spores. Leaves from inoculated plants were collected 5 d.p.i. and stained with Trypan blue. For Col-0, Est-1 and transgenic derivatives, conidiophore density was determined by dividing the total number of conidiophores present on the adaxial side of a leaf by total leaf area, which was measured using ImageJ (<http://rsbweb.nih.gov/ij/>). To assess susceptibility to *G. orontii* in a set of 96 accessions²³, spontaneous infection in a greenhouse with heavy pathogen load was exploited. Ten plants for each strain were monitored for 40 days, and arbitrarily divided into four classes of susceptibility.

Golovinomyces cichoracearum UCSC1 (ref. 45) was propagated on squash plants for 10 to 12 days and then applied to *A. thaliana*. Plants were grown in a phytochamber under short days (9 h light), at 20 °C and 60% humidity. For inoculation, an 85-cm-tall settling tower was placed over the 4- to 5-week-old *A. thaliana* plants and five to eight highly infected squash leaves were tapped over the top of the settling tower⁴⁶.

For *Hyaloperonospora arabidopsisidis* isolate Noco2, plants were grown in a phytochamber under short days (9 h light), at 22 °C during the day and 18 °C during the night. Ten-day-old seedlings or 4-week-old plants were spray-inoculated with 50,000 spores ml⁻¹ (in water). Sporangiophores were counted on seedlings at 5 d.p.i. as described^{47,48}. Adult leaves were stained with Trypan blue at 7 d.p.i. to visualize cell death and hyphal growth.

For the common peach aphid, *Myzus persicae*, plants were grown on soil in a phytochamber at 20 °C, 12 h light. Aphid proliferation was assessed by placing two alate females on three or four replicates of each of 96 plant genotypes and counting the number of offspring 9 days later.

For *Pseudomonas syringae* pv. tomato DC3000, plants were grown on soil in a phytochamber at 20 °C, 12 h light. To generate the inoculation solution, bacteria were streaked on King's B medium⁴⁹. A single colony was transferred to liquid media, which was shaken in an incubator for 24 h at 28 °C. A 1:10 dilution of the solution was then incubated for 8 h. A 1-ml aliquot was removed and pelleted in an Eppendorf tube at 2,040 g. The pellet was re-suspended in 1 ml of 10 mM MgSO₄, vortexed, and diluted to the inoculation concentration of 5×10^4 colony-forming units (c.f.u.) ml⁻¹. The seventh leaf on each of 20 replicate plants of each genotype was injected with 0.1 ml of the inoculation solution using blunt syringes⁵⁰. At 4 d.p.i., a disk was removed by hole-punch, surface-sterilized in 70% ethanol for 5 s, dried with a sterile paper towel, and ground in a 1.5-ml centrifuge tube containing 200 μl 10 mM MgSO₄ buffer. The homogenate was diluted 1:1,000 and 1:100,000 in buffer. A 50 μl aliquot of each dilution was spread on plates containing King's B medium and incubated for 2 days at 28 °C. Colony number was multiplied by 20 and the dilution factor to determine leaf bacterial titre⁵⁰.

Metabolite measurements. These were carried out independently in the Bergelson and Traw laboratories. In the Bergelson laboratory, previously published methods⁵¹ were modified to enable high-throughput extraction using two 2.3-mm Zirconia beads, 1.4-ml ScreenMate tubes and a Spex Geno/Grinder 2010. All LC/MS analyses were performed on an Agilent Technologies 1200 SL high-performance liquid chromatography (HPLC) system connected to a 6410 triple quadrupole mass spectrometer. Deuterated benzoic-D5 acid was used as an internal standard. Jasmonic acid, salicylic acid, camalexin and benzoic-D5 acid were quantified in positive ion mode using the quasi-molecular ion transitions [M+H]⁺ 211 > 151 and 211 > 165 (JA), 139 > 121 and 139 > 93 (salicylic acid), 202 > 117 (camalexin) and 128 > 82.4 (benzoic-D5 acid). Salicylic-acid glucoside was quantified in negative ion mode using the [M-H]⁻ transition 299 > 136.8.

The chromatographic method included an Eclipse-XDB C18 (Agilent) column (4.6 × 50 mm 1.8 μm) using gradient elution with 0.1% HOAc in water (A) and MeCN (B) under a flow rate of 800 μl min⁻¹. The gradient increase of solvent B was as follows: time (min)/solvent B (MeCN)/flow (ml): 0/30%/0.8; 2.7/100%/0.8; 3.7/100%/0.8; 3.71/30%/0.8; 7/30%/0.8.

In the Traw laboratory, fresh leaves were flash frozen in liquid nitrogen and stored at -80 °C. To increase sample volume, three leaves were pooled and a total of eight samples were analysed per genotype. Extraction and analysis followed a

standard protocol⁵². Approximately 100 mg of tissue was weighed, pulverized and suspended in 3 ml of 90% methanol. An internal control of 1 µg of O-anisic acid (Sigma-Aldrich) was added to each sample tube (100 µl of a 10 µg ml⁻¹ solution in 100% methanol), which was vortexed to re-suspend the tissue. Tubes were rocked in a shaker at room temperature for 24 h. The liquid was transferred to a new tube and the pellet re-suspended in 3 ml of 100% methanol, vortexed and rocked again for 24 h. The supernatant fractions were combined, the sample was split into equal volumes in two screw cap tubes, and tubes were placed in the front of a fume hood until dry (roughly 24 h later). One volume received 40 U of β-glucosidase enzyme (Sigma-Aldrich) in 400 µl of 100 mM sodium acetate buffer (pH 5.5), which cleaves the sugar from salicylic acid glucoside, thus providing an estimate of total salicylic acid present in the sample (free plus glucoside). The other volume received the 400 µl buffer, but no enzyme. All samples were incubated overnight at 37 °C, after which 400 µl of 10% trichloroacetic acid was added. Samples were then partitioned twice with 1 ml of an organic extraction solvent (100:99:1 of ethylacetate:cyclopentane:2-propanol), and vortexed each time before collecting the two organic phase fractions in a centrifuge tube. Tubes were placed in a fume hood until dry (24–48 h). Samples were re-suspended in 600 µl of 55% methanol, vortexed and placed in a rocker overnight. After centrifugation at 5,000g for 15 min, the supernatant was transferred to 0.2 µm nylon spin-prep membrane filters (Thermo Fisher Scientific) and centrifuged at 10,000g for 5 min.

Concentrations of salicylic acid were measured by HPLC on an HP1100 system with a 4.6 × 150 mm Eclipse XDB C-18 column and fluorescence detector (Agilent Technologies) with excitation at 301 nm and emission at 412, 386 and 365 nm for salicylic acid, camalexin and O-anisic acid, respectively. Solvent flow was 1 ml min⁻¹, beginning at 30% of 100% methanol and 70% of 0.5% acetic acid for 5 min, increasing to 40% methanol at 7.5 min and 60% methanol at 18 min, returning to 30% methanol at 21 min. Concentrations of salicylic acid and camalexin (µg g⁻¹ fresh weight) were calculated as the peak area of the compound divided by the product of the peak area of O-anisic acid and sample mass.

Genome-wide association studies. The biological material, SNP markers and statistical methods are described in detail in the accompanying article²⁴.

Tübingen area accessions. A set of 890 plants collected around Tübingen²⁵ was genotyped with primers that distinguished between Col-0-like and Est-1-like alleles of *ACD6*, and with a primer pair specific for KZ-10-like alleles (Supplementary Table 7b). Genotyping for Est-1-like alleles was confirmed in a subset of 384 individuals using a CAPS⁵³ marker (Supplementary Table 7b).

31. Warthmann, N., Fitz, J. & Weigel, D. MSQT for choosing SNP assays from multiple DNA alignments. *Bioinformatics* 23, 2784–2787 (2007).
32. Koch, E. & Slusarenko, A. *Arabidopsis* is susceptible to infection by a downy mildew fungus. *Plant Cell* 2, 437–445 (1990).

33. Ossowski, S., Schwab, R. & Weigel, D. Gene silencing in plants using artificial microRNAs and other small RNAs. *Plant J.* 53, 674–690 (2008).
34. Hellens, R. P., Edwards, E. A., Leyland, N. R., Bean, S. & Mullineaux, P. M. pGreen: a versatile and flexible binary Ti vector for *Agrobacterium*-mediated plant transformation. *Plant Mol. Biol.* 42, 819–832 (2000).
35. Weigel, D. & Glazebrook, J. *Arabidopsis: A Laboratory Manual* (Cold Spring Harbor Laboratory Press, 2002).
36. Lempe, J. et al. Diversity of flowering responses in wild *Arabidopsis thaliana* strains. *PLoS Genet.* 1, e6 (2005).
37. Platt, A. et al. The scale of population structure in *Arabidopsis thaliana*. *PLoS Genet.* 6, e1000843 (2010).
38. Larkin, M. A. et al. Clustal W and Clustal X version 2.0. *Bioinformatics* 23, 2947–2948 (2007).
39. Suyama, M., Torrents, D. & Bork, P. PAL2NAL: robust conversion of protein sequence alignments into the corresponding codon alignments. *Nucleic Acids Res.* 34, W609–W612 (2006).
40. Edgar, R. C. MUSCLE: multiple sequence alignment with high accuracy and high throughput. *Nucleic Acids Res.* 32, 1792–1797 (2004).
41. Thornton, K. *libsequence*: a C++ class library for evolutionary genetic analysis. *Bioinformatics* 19, 2325–2327 (2003).
42. Yang, Z. PAML 4: phylogenetic analysis by maximum likelihood. *Mol. Biol. Evol.* 24, 1586–1591 (2007).
43. Paradis, E., Claude, J. & Strimmer, K. APE: Analyses of phylogenetics and evolution in R language. *Bioinformatics* 20, 289–290 (2004).
44. Hirata, T. & Takamatsu, S. Nucleotide sequence diversity of rDNA internal transcribed spacers extracted from conidia and cleistothecia of several powdery mildew fungi. *Mycoscience* 37, 283–288 (1996).
45. Adam, L. & Somerville, S. C. Genetic characterization of five powdery mildew disease resistance loci in *Arabidopsis thaliana*. *Plant J.* 9, 341–356 (1996).
46. Vogel, J. & Somerville, S. Isolation and characterization of powdery mildew-resistant *Arabidopsis* mutants. *Proc. Natl Acad. Sci. USA* 97, 1897–1902 (2000).
47. Holt, B. F. III et al. An evolutionarily conserved mediator of plant disease resistance gene function is required for normal *Arabidopsis* development. *Dev. Cell* 2, 807–817 (2002).
48. Kaminaka, H. et al. bZIP10-LSD1 antagonism modulates basal defense and cell death in *Arabidopsis* following infection. *EMBO J.* 25, 4400–4411 (2006).
49. King, E. O., Ward, M. K. & Raney, D. E. Two simple media for the demonstration of pyocyanin and fluorescin. *J. Lab. Clin. Med.* 44, 301–307 (1954).
50. Jakob, K. et al. *Pseudomonas viridisflava* and *P. syringae*—natural pathogens of *Arabidopsis thaliana*. *Mol. Plant Microbe Interact.* 15, 1195–1203 (2002).
51. Segarra, G., Jauregui, O., Casanova, E. & Trillas, I. Simultaneous quantitative LC-ESI-MS/MS analyses of salicylic acid and jasmonic acid in crude extracts of *Cucumis sativus* under biotic stress. *Phytochemistry* 67, 395–401 (2006).
52. Dewdney, J. et al. Three unique mutants of *Arabidopsis* identify *eds* loci required for limiting growth of a biotrophic fungal pathogen. *Plant J.* 24, 205–218 (2000).
53. Konieczny, A. & Ausubel, F. M. A procedure for mapping *Arabidopsis* mutations using co-dominant ecotype-specific PCR-based markers. *Plant J.* 4, 403–410 (1993).